

# Fast neural-net based fake track rejection

Michel DeCian<sup>1</sup>, Stephen Farry<sup>2</sup>, Paul Seyfert<sup>3</sup>, Sascha Stahl<sup>4</sup>.

<sup>1</sup>*Physikalisches Institut, Ruprecht-Karls-Universität Heidelberg, Heidelberg, Germany*

<sup>2</sup>*Oliver Lodge Laboratory, University of Liverpool, Liverpool, United Kingdom*

<sup>3</sup>*Sezione INFN di Milano Bicocca, Milano, Italy*

<sup>4</sup>*European Organization for Nuclear Research (CERN), Geneva, Switzerland*

## Abstract

A neural-network based algorithm to identify fake tracks in the LHCb pattern recognition is presented. This algorithm, called ghost probability, is fast enough to fit into the CPU time budget of the software trigger farm. It allows reducing the fake rate and consequently the combinatorics of the decay reconstructions, as well as the number of tracks that need to be processed by the particle identification algorithms. As a result, it strongly contributes to the achievement of having the same reconstruction online and offline in the LHCb experiment.



# 1 Introduction

The LHCb detector consists of subsystems designed to perform high efficiency tracking ( $> 95\%$ ) with an excellent momentum resolution ( $0.5\%$  for  $p < 20 \text{ GeV}/c$ ). Two Ring Imaging Cherenkov detectors provide precise particle identification. In Run II of the LHC, a new scheme for the LHCb software trigger allows splitting the triggering of the event in two stages, giving room to perform the alignment and calibration in real time. In the novel detector alignment and calibration strategy for Run II, data collected at the start of the fill are processed in a few minutes and used to update the alignment, while the calibration constants are evaluated for each run. This allows identical constants to be used in the online and offline reconstruction.

One of the challenges to achieve run the offline reconstruction in the software trigger is the limited CPU time budget of the computing farm. The reconstruction time of events depends strongly on the number of reconstructed charged particle tracks in an event in two ways. The particle identification (PID) is evaluated for every reconstructed track in the second stage of the software trigger; and the combinatorics of reconstruction decay vertices gets more complex with more reconstructed tracks.

A key ingredient to fit the offline reconstruction into the software trigger is the reduction of the fake track rate prior to the PID and combinatorics of reconstructing particle decays in the second software trigger stage. A neural network, described in this note, is deployed to identify fake tracks, called the “ghost probability”.

Without applying the ghost probability, the RICH PID is about  $5\%$  of the entire trigger CPU budget, roughly  $3\%$  of the CPU budget is spent on decay combinatorics, and  $15\%$  of all events which enter the software trigger are processed by both software trigger stages.

## Terminology

To avoid ambiguity, the bare term “performance” is avoided. Instead, when referring to how well good tracks are separated from fake tracks, the term “physics performance” is used since it is the figure of merit on which physics analyses depend. The term “CPU performance” is used for the amount of computing resources needed to execute the algorithm proposed in this note. As benchmark for the latter, the cycle count of callgrind [1] is used. Effects of instruction caching and data caching are assumed small, approximately confirmed by wall clock time measurements. The cycles spent in other algorithms which are only called to compute input quantities to the ghost probability are accounted to the ghost probability, most notably this comprises the interpolation of tracks through active detector material to determine which channels should have a hit from the track – algorithms like the track fit, which would be executed anyways, are not accounted to the ghost probability.

The term “ghost probability” is used for both, the entire algorithm computing whether a track is considered a fake track or a real track, including the neural network, and for the numeric response of that algorithm. When the ghost probability is referred to as a

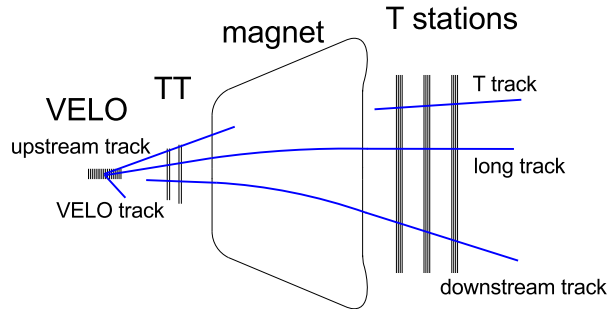


Figure 1: Illustration of the tracking system of LHCb, starting from the VELO around the collision point on the left, particles pass the TT, are deflected in the magnetic field of the dipole magnet and then detected in the T station detector (IT and OT). Different track types are reconstructed by different track finding algorithms. [2]

41 selection requirement, the nominal working point of 0.4 is implied, corresponding to a fake  
 42 track retention of 40 %.

### 43 1.1 Track reconstruction

44 Owing to the design of the LHCb detector, which consists of tracking detectors mainly  
 45 outside the magnetic field, charged particle tracks are in approximation straight line  
 46 segments in the upstream part (VELO and TT) and in the downstream part (T stations).  
 47 Figure 1 shows an overview of the different track types defined in the LHCb reconstruction:  
 48 VELO tracks, which have hits in the VELO only; upstream tracks, which have hits in  
 49 the two upstream trackers; T tracks, which have hits in the T stations only; downstream  
 50 tracks, which have hits in TT and the T stations; and long tracks, which have hits in the  
 51 VELO and the T stations. The latter tracks can additionally have hits in TT.

52 If a particle is reconstructed more than once, as different track types, only the track  
 53 best suited for analysis purposes is kept. Hereby, long tracks are preferred over any other  
 54 track type, upstream tracks are preferred over VELO tracks, and downstream tracks are  
 55 preferred over T tracks.

56 Most analyses use long tracks because they provide the best momentum and spatial  
 57 resolution among all track types. Unless otherwise stated, track reconstruction at LHCb  
 58 refers to the reconstruction of long tracks. In a typical signal triggered event, around 60  
 59 long tracks are reconstructed. Other track types, such as downstream tracks, are used  
 60 for the reconstruction of decay products of long-lived particles such as  $K_s^0$  mesons, or for  
 61 internal alignment of the tracking detectors.

62 Tracks are fit with a Kalman filter fit. In addition to a global fit  $\chi^2$ , separate  
 63 contributions to the  $\chi^2$  from the downstream detectors (IT and OT),  $\chi_D^2$ , and from the  
 64 upstream detectors (VELO and TT),  $\chi_U^2$  are computed. A large number of fake tracks  
 65 results from wrong combinations of well reconstructed track segments in the upstream and  
 66 downstream regions. These usually have good  $\chi_D^2$  and  $\chi_U^2$  but the additional contribution

67 from matching the two segments,  $\chi_M^2 = \chi^2 - \chi_D^2 - \chi_U^2$ , is large for these “matching” fakes.

68 The Kalman fit has an outlier removal to account for individual detector hits which are  
 69 not due to the reconstructed particle track. Beyond that, a special treatment for Outer  
 70 Tracker hits is in place. The readout electronics is designed to select only a single hit in  
 71 each channel per bunch crossing; if two charged particles pass the same straw, a drift time  
 72 measurement will only be provided for one of them. To describe tracks in high occupancy  
 73 OT modules, the drift time measurement can be ignored and only the information that  
 74 a track went somewhere through the straw is used. This is decided for each straw–track  
 75 combination individually if the hit residual is too large, similar to a standard outlier  
 76 removal. This drift time suppression ensures that the track fit  $\chi^2$  is not biased to larger  
 77 values for tracks in high multiplicity events, for tracks in the OT with respect to tracks in  
 78 the IT, or for tracks in high occupancy modules, which are those closer to the beam axis.

## 79 1.2 Previous works

80 An earlier version of the work presented here, referred to as old ghost probability, was  
 81 already used in analyses of Run I data. The neural network was evaluated in the offline  
 82 reconstruction to distinguish fake tracks from real particles’ tracks [3] (used e.g. in [4]).  
 83 The network was trained on all reconstructed tracks in simulated events with at least one  
 84  $b\bar{b}$  pair produced in the  $pp$  collision.

85 The 22 input variables to the old ghost probability are the track fit  $\chi^2$ , and the individual  
 86 contributions  $\chi_D^2, \chi_U^2, \chi_M^2$  and the corresponding degrees of freedom; the numbers of hits  
 87 on the track in each tracking detector; the reconstructed track  $p_T$  and pseudorapidity; the  
 88 difference in the number of observed hits on a track and the “expected hits”, calculated  
 89 interpolating the track through the detector and counting how many active strips/straws  
 90 the track passes through; and finally the occupancies of all tracking detectors.

91 There are separate networks for each track type, where input variables are removed if  
 92 they are not defined for that track type (e.g. VELO hits for downstream tracks).

## 93 1.3 Network architecture tuning

94 As framework for the neural network, the TMVA package [5] is chosen since it is

- 95 • equipped with a root file interface for the training, which is the common data file  
 96 format in LHCb software,
- 97 • commonly known in LHCb (ensuring future maintainability),
- 98 • able to provide code generation for the trained network such that the network can  
 99 be integrated into any C++ code without creating dependency on external libraries.

100 Mathematically, the shallow neural network that is implemented a composed function

$$\mathbb{R}^n \xrightarrow{\text{linear} + \text{const}} \mathbb{R}^m \xrightarrow{\text{element wise non-linear}} \mathbb{R}^m \xrightarrow{\text{linear} + \text{const}} \mathbb{R} \xrightarrow{\text{non-linear}} \mathbb{R}.$$

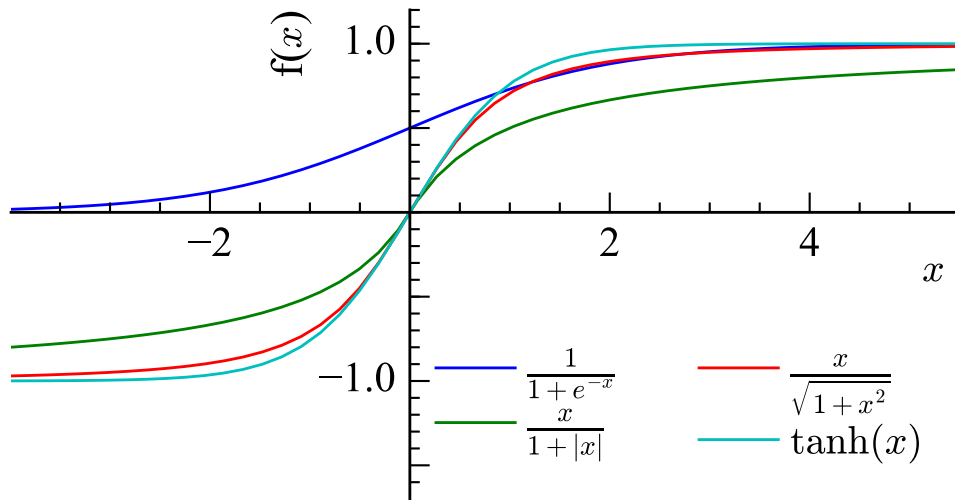


Figure 2: Functional shape of sigmoid functions.

101 The entries of the matrices for the linear mappings ( $(n+1) \times m$  for the first and  $(m+1)$   
 102 for the second) are subject to optimisation, where  $n$  is the number of input variables and  
 103  $m$  chosen as  $n+5$ . The non-linearities, so-called activation functions, are fixed real valued  
 104 functions.

105 At the time of development, the  $\tanh(x)$  function was a commonly used activation  
 106 function in TMVA, while known as a computationally expensive function to be optimised  
 107 for the LHCb pattern recognition [6]. Yet it is not the only possible sigmoid function [7]  
 108 and consequently custom activation functions have been added to TMVA [8].

109 Of the tested functions  $\frac{x}{\sqrt{1+x^2}}$  is the fastest to compute, while no significant physics  
 110 performance difference is expected given the similar functional shape, see Fig. 2. Indeed,  
 111 no performance difference is observed in Fig. 3. Therefore, it is chosen as activation  
 112 function.

113 The ghost probability is a classification problem, and thus cross entropy [9] is chosen  
 114 as loss function in the network training. With respect to the run I implementation of the  
 115 ghost probability, this contributes to the physics performance improvement. The activation  
 116 function of the output layer is  $\frac{1}{1-e^{-x}}$  in the training. In the application, a custom output  
 117 calibration is applied instead, as described in Sect. 1.5).

## 118 1.4 Variable selection

119 To allow for enough development time for testing and evaluation, the selection of input  
 120 variables is mostly unchanged from Run I with two exceptions. The track interpolation to  
 121 determine the number of expected hits is removed to reduce the CPU usage of the ghost  
 122 probability by a factor 10. The number of track candidates competing for shared hits in  
 123 the pattern recognition is added as input variable.

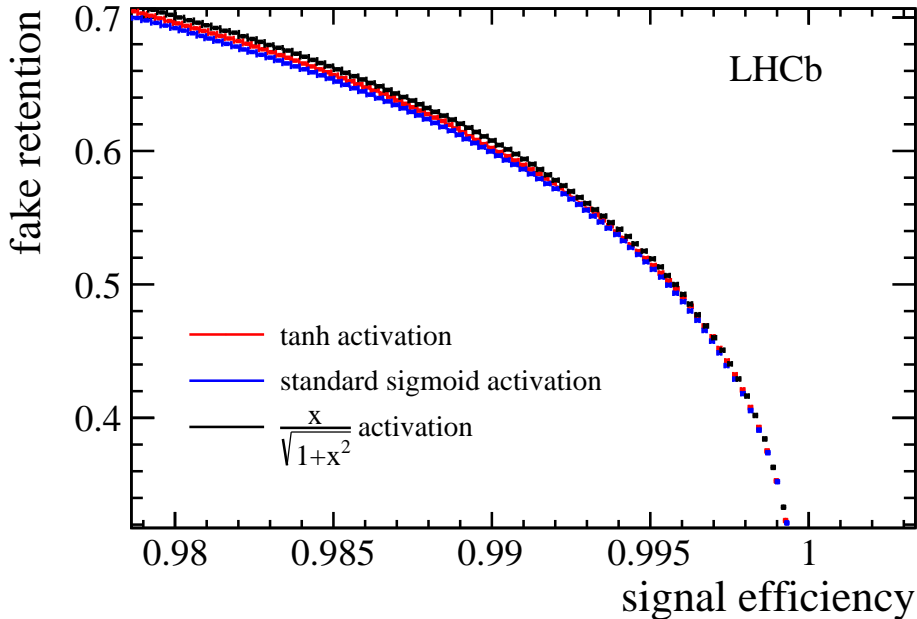


Figure 3: ROC curves for fake track discriminating neural networks, using different activation functions. A very small physics performance improvement is observed when changing from the TMVA standard functions to  $\frac{x}{\sqrt{1+x^2}}$ .

## 124 1.5 Output transformation

125 To ease the usage of the ghost probability, a transformation of the network response is  
 126 applied. A probability integral transform – also referred to as “flattening” or “rarity  
 127 transformation” – is obtained as a linear spline fit to the cumulative network response for  
 128 fake tracks in simulated events. The discriminating behaviour of any classifier is invariant  
 129 under monotonous transformations and so is the physics performance under the probability  
 130 integral transform. Motivations for this transformation are primarily to give a physical  
 131 interpretation to the response: rejecting tracks with a ghost probability of larger than  $x\%$   
 132 will retain  $x\%$  of all fake tracks.

133 In addition any update of the ghost probability training will have the same behaviour  
 134 and thus the optimal working points of algorithms downstream of the ghost probability  
 135 algorithm will remain unchanged at leading order.

## 136 1.6 Category classifiers

137 Fake tracks produced by different pattern recognition algorithms might have different  
 138 track properties. It might therefore be beneficial to train separate neural networks for  
 139 the two main track reconstruction algorithms at LHCb. On simulated events, the physics  
 140 performance of two separate networks does not differ from the physics performance of a  
 141 single network. Similarly, different networks for different T station regions have been tested

142 (one for tracks in the OT, IT, and the overlap region), without significant performance  
143 gain. We suspect reasons are twofold. Firstly, the network already knows which T station  
144 tracker a track went through due to the hit counts in the individual subdetectors. Secondly,  
145 for the different algorithms, we suspect the common track fit is more indicative for whether  
146 a track is a fake or not, than the pattern recognition strategy.

147 Consequently, a single network for all pattern recognition algorithms in the entire  
148 detector is deployed.

## 149 1.7 Training sample

150 The LHCb track reconstruction needs to be able to handle a wide range of LHC running  
151 conditions. At the time of preparing for data taking in 2015 it was not clear whether the  
152 LHC would operate at 25 ns bunch spacing or 50 ns bunch spacing. Simulations to prepare  
153 the track reconstruction were prepared for these scenarios:

- 154 • 25 ns bunch spacing,  $\nu = 1.6$
- 155 • 25 ns bunch spacing,  $\nu = 1.9$
- 156 • 50 ns bunch spacing,  $\nu = 1.6$
- 157 • 50 ns bunch spacing,  $\nu = 2.7$

158 where  $\nu$  is the average number of  $pp$  interactions per bunch crossing.

159 The scenarios differ, for what concerns the track reconstruction, significantly in detector  
160 occupancy and spillover in the Outer Tracker. That may lead to different behaviours  
161 of fake track reconstruction and require different network trainings for different running  
162 conditions. The necessity for having different network trainings is assessed by training  
163 networks for each of the running conditions, with all other training parameters fixed,  
164 and evaluating the networks on one of the samples and their discriminating powers are  
165 compared. Figure 4 shows the ROC curves for the 25 ns sample at low pile-up. The  
166 discrimination powers of the four networks do not largely differ and thus for simplicity only  
167 a single network (trained at the favoured scenario of 25 ns bunch spacing at low pile-up) is  
168 deployed.

## 169 2 Validation

170 The data taking strategy of LHCb in Run II involves the application of the same track  
171 reconstruction in the software trigger as in the offline data processing. This goal can  
172 only be achieved within the time constraints of the software trigger by applying the ghost  
173 probability in the trigger. This ghost probability reduces the rate of fake tracks entering  
174 the particle identification and combinatorics of decay reconstructions and thereby saves  
175 more time than the computation of the ghost probability.

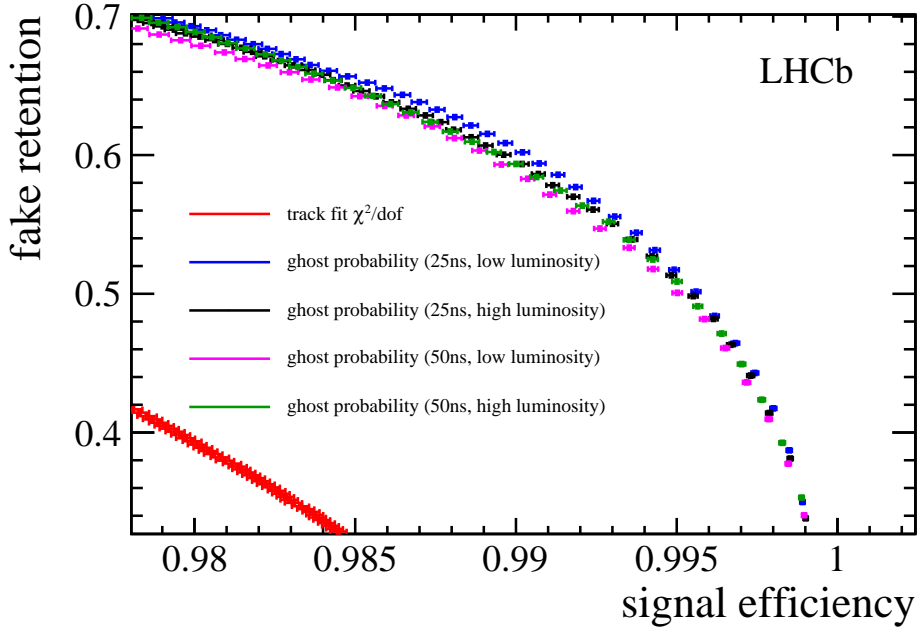


Figure 4: ROC curves for fake track discriminating neural networks (blue, black, magenta, and green), trained for different LHC running conditions, evaluated for 25 ns bunch spacing,  $\nu = 1.6$ . The red points are the ROC curve for the track fit reduced  $\chi^2$ , which performs significantly worse than any of the neural networks.

176 It must therefore be ensured that the full physics program of LHCb can be done with  
 177 tracks passing the ghost probability, and that there is no corner of phase space or particle  
 178 species, which is rejected by the ghost probability.

179 The computation of the track fit  $\chi^2$  was last revised in 2015 between data taking  
 180 at 50 ns and 25 ns bunch spacing, [10]. For conclusive validations, tracks in Run I data  
 181 and from 2015 data with 50 ns bunch spacing are refitted before computing the ghost  
 182 probability.

## 183 2.1 High momentum tracks

184 Due to their low cross section, tracks in the momentum range of  $Z \rightarrow \mu\mu$  events are absent  
 185 in the training data. This could lead to a low selection efficiency for very high momentum  
 186 tracks.

187 In the early measurement period in 2015 at a bunch spacing of 50 ns, the nominal 2015  
 188 pattern recognition was used without application of the ghost probability. Refitting the  
 189 candidate tracks from  $Z \rightarrow \mu\mu$  decays in that period allows to assess the performance of  
 190 the ghost probability for very high momentum tracks. The measured efficiency in Fig. 5  
 191 shows that the absence of very high momentum tracks does not lead to a low efficiency.

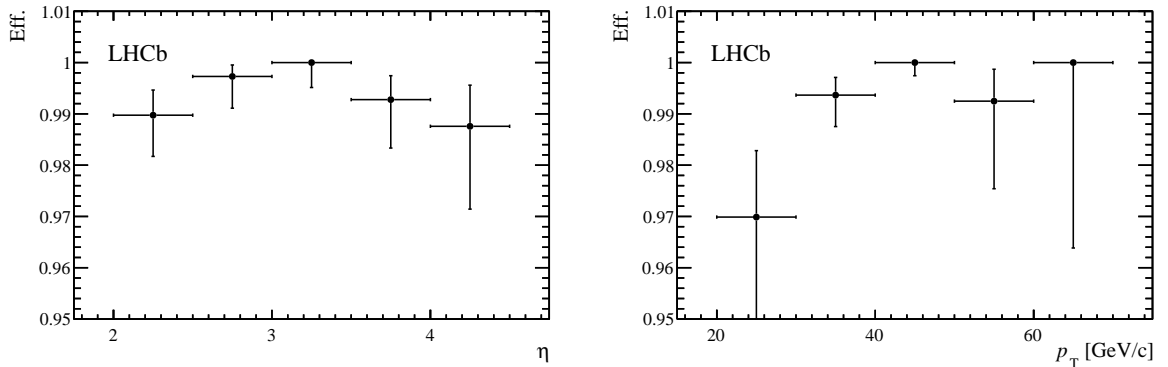


Figure 5: Efficiency for  $Z \rightarrow \mu\mu$  tracks to pass the ghost probability, in data from 2015 at a bunch spacing of 50 ns.

## 2.2 Electron reconstruction

192

193 Electrons are more challenging to reconstruct than the standard candles ( $Z \rightarrow \mu\mu$  or  
 194  $D \rightarrow K\pi$ ). At the same time, it can be expected that the response of the ghost probability  
 195 for electrons differs from that for other particles as electrons undergo more multiple  
 196 scattering.

197 It is assumed that the reconstruction of converted photons as electron pair is the most  
 198 vulnerable part for the following reasons. The photon conversion can happen “late” in the  
 199 VELO leaving only few hits. In addition, the  $e^+e^-$  pair has a small opening angle which  
 200 could lead to hit ambiguities in the VELO pattern reconstruction. It should be noted that  
 201 analyses of channels like  $B_s^0 \rightarrow K^*\gamma$  are anyhow so-called rare decays which immediately  
 202 suffer from efficiency loss.

203 The “early data” of 2015 does not correspond to enough integrated luminosity to  
 204 obtain a satisfying estimation of the consequences of a cut on the ghost probability on  
 205 converted photons. For this reason, the tracks of  $B_s^0 \rightarrow K^*\gamma$  candidates from Run I – using  
 206 a simplified version of the selection presented in [11] without Bremsstrahlungs correction –  
 207 are refitted using the track fit configuration as used in 2015 and the ghost probability is  
 208 evaluated. The invariant mass spectrum shown in Fig. 6 shows candidates without the  
 209 application of a cut on the ghost probability, those passing, and those failing; both for  
 210 converted photons reconstructed as pair of downstream tracks and as pair of long tracks.  
 211 To the statistical precision of this test, no signal loss is visible.

## 2.3 Validation with 25 ns data

212

213 A cut on the ghost probability is included in the standard track reconstruction since data  
 214 taking at 25 ns bunch spacing started. To investigate the behaviour of the ghost probability  
 215 in real data with 25 ns bunch spacing, events are re-reconstructed without a cut on the  
 216 ghost probability. Under the assumption, that most  $K_s^0$  are part of the underlying event  
 217 and most triggered events containing  $K_s^0$  would have been triggered without those  $K_s^0$ ,  $K_s^0$

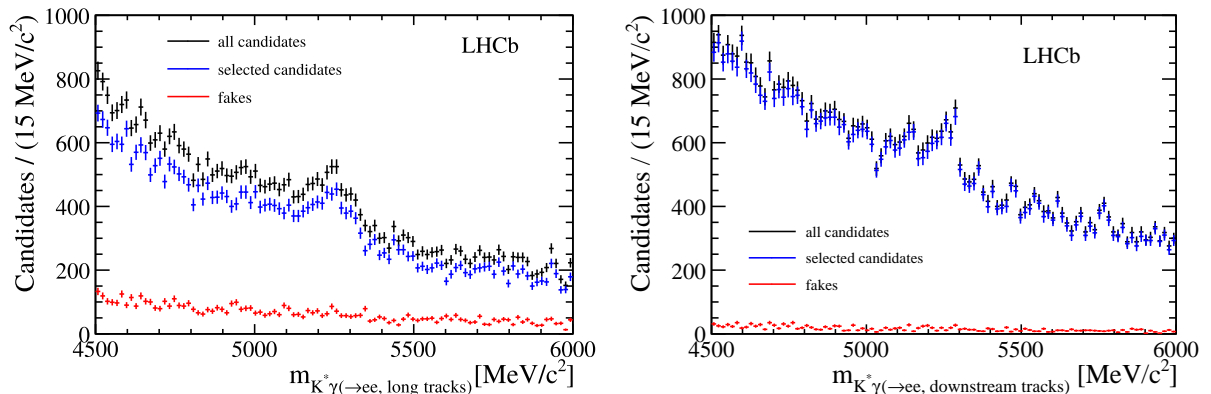


Figure 6:  $B_s^0 \rightarrow K^* \gamma$  candidates, where the photon is reconstructed as pair of electron tracks, using long tracks (left) and using downstream tracks (right). The candidates prior to a cut on the ghost probability of the electron tracks are shown in black, those passing the ghost probability in blue, and those candidates rejected by the ghost probability in red. No signal loss is visible in the rejected candidates.

218 are used as probe of the ghost probability.

219 The invariant mass spectrum of  $K_s^0$  candidates after re-reconstruction is shown in  
 220 Fig. 7 for both long tracks and downstream tracks. In both cases,  $K_s^0$  candidates are  
 221 reconstructed from two opposite charged pions which are compatible with originating  
 222 from a common vertex, which satisfy fiducial momentum requirements, and which are  
 223 significantly displaced from any primary collision vertex. In either case, the background  
 224 contribution is largely reduced when rejecting events where at least one of the tracks has  
 225 a ghost probability of larger than 0.4. There is no signal visible in the events rejected. It  
 226 is concluded that no physics signal is lost due to the application of the ghost probability  
 227 within the statistical sensitivity of the test in the kinematic spectrum of the selected  $K_s^0$ .

228 The same test with  $D \rightarrow K \pi$  decays is shown in Fig. 8 on the right. Similar to the  $K_s^0$   
 229 selection, kaon and pion tracks are selected with minimal momentum requirements and  
 230 are required to originate from a common, displaced vertex. Additionally, the kaon track  
 231 must be identified as kaon by the RICH system. To ensure that the sample is not biased  
 232 towards candidates passing the ghost probability due to the online event selection, the  
 233 ghost probability spectrum is shown in Fig. 8 b), where no step from such a selection is  
 234 visible at 0.4.

## 235 2.4 Decay time acceptance

236 The study of long lived particles ( $b$  and  $c$  hadrons) is the major part of the LHCb physics  
 237 program. It must therefore be ensured that the ghost probability does not reject particles  
 238 from displaced vertices at a higher probability than particles from primary collisions (which  
 239 have a higher prevalence in the training).

240 To evaluate a possible decay time bias of the ghost probability, for each reconstructed

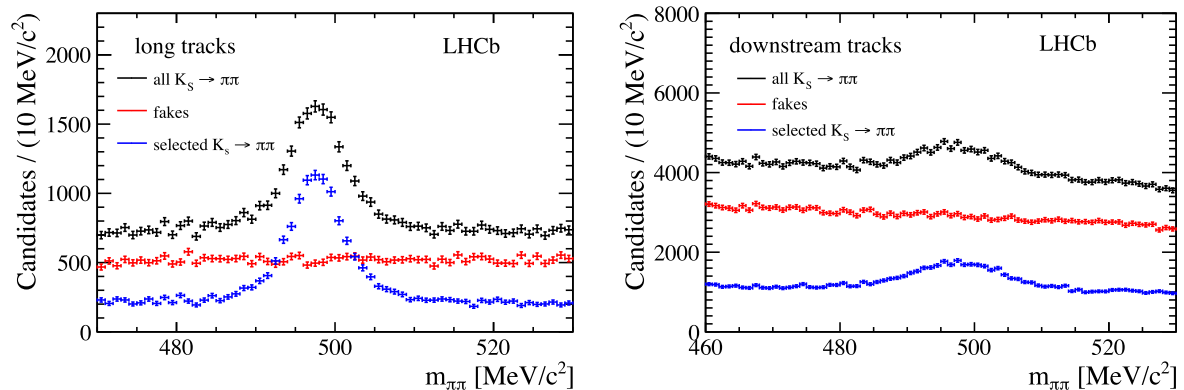


Figure 7:  $K_S^0 \rightarrow \pi\pi$  invariant mass spectrum for events reconstructed without using the ghost probability in the track selection; using long tracks (left) and downstream tracks (right). Candidates for which at least one track fails the default ghost probability requirement are shown in red and do not exhibit a signal contamination. The remaining candidates are shown in blue.

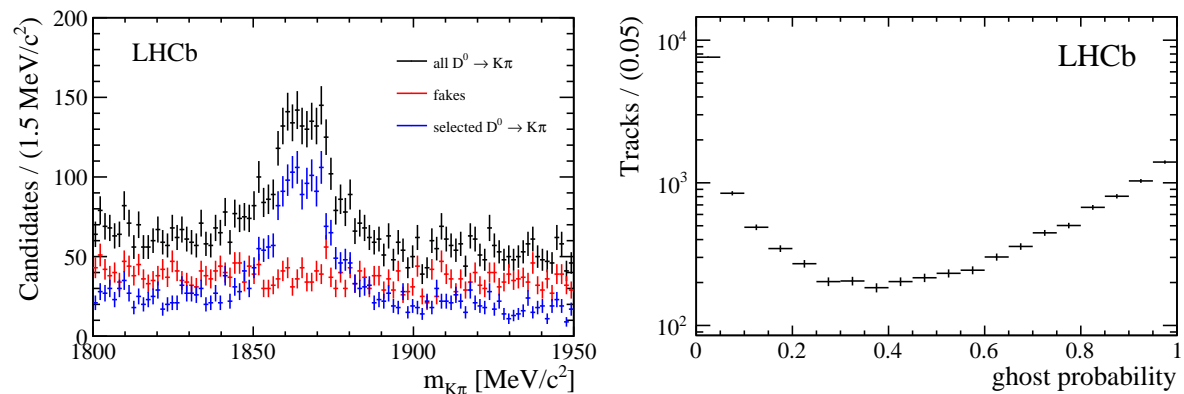


Figure 8:  $D \rightarrow K\pi$  invariant mass spectrum for events reconstructed without using the ghost probability in the track selection (left). Candidates for which at least one track fails the default ghost probability requirement are shown in red and do not exhibit a signal contamination. The remaining candidates are shown in blue. The ghost probability distribution for the kaon and pion tracks is shown on the right.

241 particle in simulated events with a  $b\bar{b}$  production, the average of the true decay time of their  
 242 ancestor particles is determined. When rejecting tracks which fail the ghost probability  
 243 criterion, the average ancestor decay time changes by  $(1.5 \pm 2.0) \times 10^{-15}$  s. This is smaller  
 244 than the statistical sensitivity of this test, and smaller than the systematic uncertainty to  
 245 which the lifetime bias of the LHCb reconstruction is known [12].

### 246 3 Impact on trigger CPU consumption

247 Applying the ghost probability in the first software trigger stage, reduces the rate of events  
248 which pass the first stage, and therefore the HLT2 reconstruction needs to reconstruct 4 %  
249 less events. In combination with the ghost probability requirement in HLT2, the RICH  
250 PID is executed for 22 % fewer tracks and the CPU reduced for it is reduced by 23 %.  
251 The combinatorics, in the example of the 2-body topologic trigger, is reduced by 69 %,  
252 resulting in 53 % fewer trigger candidates. The CPU consumption for combinatorics for  
253 all trigger lines is reduced by 58 %.

254 The evaluation of the ghost probability itself “costs” 0.2 % of the HLT CPU budget  
255 (in roughly equal parts for HLT1 and HLT2), which underlines the overall benefit of its  
256 application.

257 For the entire software trigger this results in a reduced CPU consumption of 16 % –  
258 assuming that roughly half of the current HTL farm costed  $\mathcal{O}(2\text{ M CHF})$ , this is equivalent  
259 to 640 k CHF.

### 260 4 Outlook

261 The current networks are trained for the track reconstruction for data taking in 2015  
262 at 25 ns bunch spacing, using the latest simulations available at the time. Retraining  
263 are advisable for significant updates in the track reconstruction “upstream” of the ghost  
264 probability (i.e. the pattern recognition and the track fit). Physics performance gains can  
265 also be expected with improved machine learning techniques or event simulations.

266 Additional separation between “good” tracks and fake tracks could be gained by using  
267 hit expectations in active layers: at the moment only the numbers of hits in the individual  
268 subdetectors on the track are used. These could be compared with the intersections of the  
269 trajectory with active detector material such that the number of missing hits is used as  
270 input for the network [13].

271 The current training is purely based on simulated events, the domain adaptation  
272 approach from [14] is not applied as it currently does not lead to an improved fake track  
273 rejection. The ghost probability network is retrained using good tracks and fake tracks  
274 from simulated events and unlabelled tracks from real events with the Caffe software  
275 framework [15], which is used in [14]. In addition to the network with domain adaptation,  
276 a conventional network is trained to disentangle effects from the training algorithm (TMVA  
277  $\rightarrow$  Caffe) and network architecture (adding a gradient reversal layer and domain classifier).  
278 This working point of the network responses is chosen to retain the same number of  $K_S^0$   
279 candidates as the application of the nominal ghost probability. From the invariant mass  
280 distribution in Fig. 9, it can be seen that the TMVA network and the two networks trained  
281 in Caffe yield close to identical physics performance; the data points of the network with  
282 domain adaptation are almost entirely covered by the data points of the Caffe network  
283 without domain adaptation. This does not rule out that domain adaptation can not  
284 improve the physics performance of the ghost probability in the future.

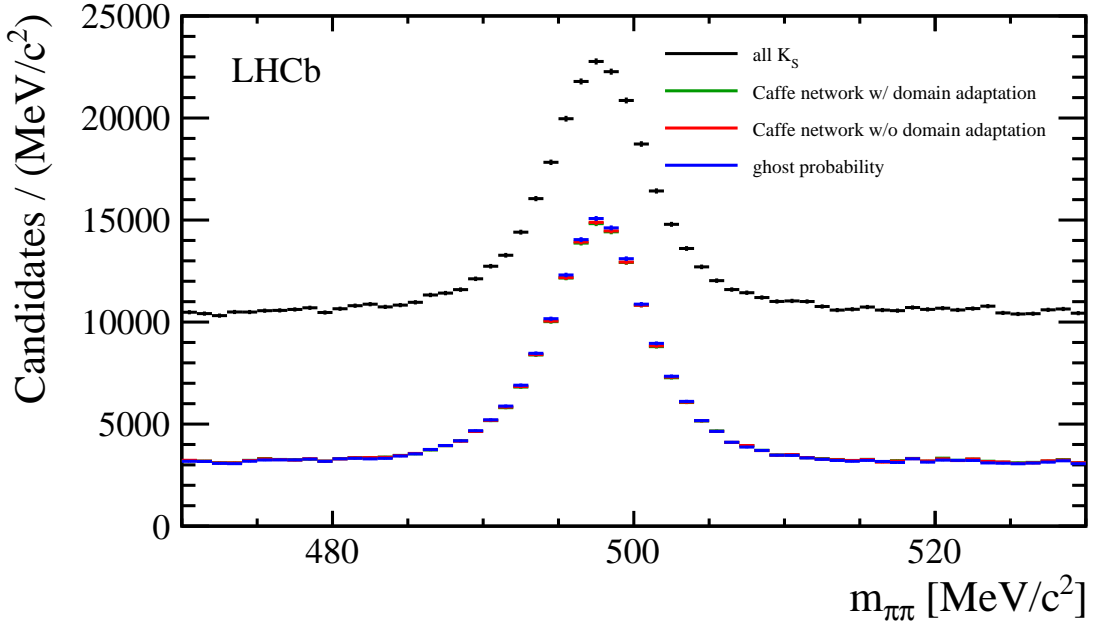


Figure 9: Comparison of the  $K_s^0$  selection with the nominal ghost probability (blue), a network trained with the Caffe package (red), and a network trained with domain adaptation (green, covered by red). The working points of the Caffe networks are chosen to retain the same numbers of candidates. Hardly any performance difference is visible.

Table 1: Callgrind benchmark comparisons of different activation functions. Fields with n/a have not been evaluated or are not available with AVX intrinsics. The activation function used by the ghost probability is marked with (\*).

function	default compiler options	AVX vectorisation by hand
$\tanh$	19,355,124,355	n/a
$\frac{1}{1+e^{-x}}$	21,140,125,632	n/a
$\frac{x}{\sqrt{1+x^2}}$ (*)	415,121,741	195,121,939
$\frac{x}{1+ x }$	395,121,798	195,104,759
$\max(0, x)$	155,095,875	115,095,891

285 The current network relies on auto-vectorisation. The methods suggested by [16] lead  
 286 to tenfold improvement of the neural network implementation [17] once using AVX intrinsic  
 287 commands. This approach has not been followed up to ensure platform independence of  
 288 the ghost probability.

289 The current activation function in the neural network is  $\frac{x}{\sqrt{1+x^2}}$ . The rectified linear  
 290 unit  $\max(0, x)$  or  $\frac{x}{1+|x|}$  are expected to be even faster, as listed in Tab. 1 (from [18]).

## 5 Conclusion

The ghost probability is introduced as a default method of reducing the number of fake tracks in the LHCb reconstruction and is deployed for offline and online reconstruction. The reduction of fake tracks in the particle identification and combinatorics of decay reconstruction greatly reduces the demand of computing resources of the software trigger and enables LHCb to use identical reconstructions online and offline. Validations at different phase space points reveal no adverse side effects of applying the ghost probability centrally.

## Acknowledgements

We express our gratitude to our colleagues in the LHCb collaboration who provided suggestions and helped in the implementation, especially Angelo Di Canto, Helge Voss, Manuel Schiller, Gerhard Raven, Chris Jones; from the Electronic Vision(s) group (Kirchhoff-Institute for Physics, Ruprecht-Karls-Universität Heidelberg, Heidelberg, Germany) Eric Müller; and from the LHC Physics and New Particles group (Institute for Theoretical Physics, Ruprecht-Karls-Universität Heidelberg, Heidelberg, Germany) Johann Brehmer.

## References

- [1] J. Weidendorfer, M. Kowarschik, and C. Trinitis, *A Tool Suite for Simulation Based Analysis of Memory Access Behavior*, in *Computational Science - ICCS 2004, 4th International Conference, Kraków, Poland, June 6-9, 2004, Proceedings, Part III* (M. Bubak, G. D. van Albada, P. M. A. Sloot, and J. Dongarra, eds.), vol. 3038 of *Lecture Notes in Computer Science*, pp. 440–447, Springer, 2004. <http://www.valgrind.org/docs/pubs.html>.
- [2] LHCb collaboration, R. Aaij *et al.*, *Measurement of the track reconstruction efficiency at LHCb*, JINST **10** (2015) P02007, [arXiv:1408.1251](https://arxiv.org/abs/1408.1251).
- [3] J. Brehmer, J. Albrecht, and P. Seyfert, *Ghost probability: an efficient tool to remove background tracks*, <https://cds.cern.ch/record/1478372>. LHCb internal note LHCb-INT-2012-025.
- [4] LHCb collaboration, R. Aaij *et al.*, *Observation of  $B_c^+ \rightarrow J/\psi D_s^+$  and  $B_c^+ \rightarrow J/\psi D_s^{*+}$  decays*, Phys. Rev. **D87** (2013) 112012, [arXiv:1304.4530](https://arxiv.org/abs/1304.4530).
- [5] A. Hoecker *et al.*, *TMVA: Toolkit for Multivariate Data Analysis*, PoS **ACAT** (2007) 040, [arXiv:physics/0703039](https://arxiv.org/abs/physics/0703039).
- [6] M. Schiller, H. Voss, and L. Moneta, *fast tanh implementation*, ROOT-7054.
- [7] Wikipedia. Sigmoid function, 2015.

- 324 [8] P. Seyfert and H. Voss, *TActivation... implementations*, ROOT-7062.
- 325 [9] C. M. Bishop, *Pattern recognition and machine learning*, Information science and  
326 statistics, Springer, New York [u.a.], 10. (corrected at 8th printing) ed., 2009; J.-H.  
327 Zhong *et al.*, *A program for the Bayesian Neural Network in the ROOT framework*,  
328 Comput. Phys. Commun. **182** (2011) 2655, [arXiv:1103.2854](https://arxiv.org/abs/1103.2854).
- 329 [10] M. Heß, *Multiple scattering in track reconstruction*,  
330 <https://cds.cern.ch/record/1957764>. LHCb internal note LHCb-INT-2014-043.
- 331 [11] L. Beaucourt, E. Tournfier, M. N. Minard, and J. F. Marchand,  $B^0 \rightarrow K^*\gamma(e^+e^-)$   
332 and  $B_s^0 \rightarrow \phi\gamma(e^+e^-)$  analysis status, in *2nd Radiative decays @LHCb Workshop*  
333 (A. Oyanguren Campos *et al.*, eds.), 2015. <https://indico.cern.ch/event/375424/>.
- 334 [12] LHCb collaboration, R. Aaij *et al.*, *Measurements of the  $B^+$ ,  $B^0$ ,  $B_s^0$  meson and  $\Lambda_b^0$*   
335 *baryon lifetimes*, JHEP **04** (2014) 114, [arXiv:1402.2554](https://arxiv.org/abs/1402.2554).
- 336 [13] W. Hulsbergen, *LHCBPS-1414*, <https://its.cern.ch/jira/browse/LHCBPS-1414>.
- 337 [14] Y. Ganin and V. Lempitsky, *Unsupervised Domain Adaptation by Backpropagation*,  
338 ArXiv e-prints (2014) [arXiv:1409.7495](https://arxiv.org/abs/1409.7495).
- 339 [15] Y. Jia *et al.*, *Caffe: Convolutional Architecture for Fast Feature Embedding*,  
340 [arXiv:1408.5093](https://arxiv.org/abs/1408.5093).
- 341 [16] V. Vanhoucke, A. Senior, and M. Z. Mao, *Improving the speed of neural networks on*  
342 *CPUs*, <https://research.google.com/pubs/archive/37631.pdf>.
- 343 [17] P. Seyfert, *github project TMVA-MLP*, <https://github.com/pseyfert/tmva-mlp>.
- 344 [18] P. Seyfert, *CPU performance comparison of activation functions*,  
345 [https://twiki.cern.ch/twiki/bin/view/Main/PaulSeyfert?forceShow=1#activation\\_function](https://twiki.cern.ch/twiki/bin/view/Main/PaulSeyfert?forceShow=1#activation_function).